15th World Congress on Computational Mechanics (WCCM-XV)
8th Asian Pacific Congress on Computational Mechanics (APCOM-VIII)
Virtual Congress: 31 July – 5 August 2022
S. Koshizuka (Ed.)

# BAYESIAN OPTIMIZATION ON FIFTH-ORDER TARGETED ENO SCHEME FOR COMPRESSIBLE FLOWS

**Yiqi Feng**[1], **Felix S. Schranner**[1], **Josef Winter**[1] **and Nikolaus A. Adams**[1]

[1] Chair of Aerodynamics and Fluid Mechanics, School of Engineering and Design
Technical University of Munich, Boltzmannstr. 15, 85748 Garching, Germany
yiqi.feng@tum.de

**Key words:** Bayesian Optimization, Gaussian Process, Targeted ENO, Riemann Solver, Implicit Large Eddy Simulation

**Abstract.** *Targeted ENO (TENO) has been proposed to overcome the shortcomings of WENO schemes, namely excessive dissipation of lower-order upwind-biased and degenerated schemes, and limited robustness of central-biased schemes. TENO offers a set of free parameters to shape the inherent effective local dissipation and dispersion. In the original formulation of TENO, these free parameters have been adjusting by means of the approximate dissipation-dispersion relation. Hence, the TENO formulation may be superior in this aspect, yet, it does not necessarily outperform other schemes in flows involving non-linear interaction of a broad range of scales. Data-driven methods enable optimizing these free parameters instead of adjusting them. In this work, we demonstrate the application of an iterative Bayesian optimization approach on designing fifth-order TENO (TENO5) schemes. Exploiting that Bayesian optimization efficiently and robustly finds an optimum of an expensive function with a low number of trials, we construct specific TENO5-schemes for compressible flows with gas dynamic discontinuities as well as for implicit large eddy simulation (ILES). For the former, we measure the error between under-resolved simulations of the Sod shock tube and its analytical solution for automatically generated TENO5 formulations as the objective. For the latter, under-resolved inviscid Taylor-Green vortex flows are evolved to their turbulent state, in which their kinetic energy spectrum in the inertial subrange is compared to the theoretical Kolmogorov-scaling solution to formulate its objective. We show that these two TENO5 formulations perform superior to the original formulation of TENO5 relevant to the specific types of flows. Also, a variety of benchmark test flows show that both specific TENO5 formulations outperform the original one in terms of phase speed, shock-preservation, as well as physical consistency of fluid-dynamic instabilities and turbulent flows.*

## 1 INTRODUCTION

When seeking to study flow structures such as strong shocks, instability phenomena or small-scale vortices, computational fluid dynamics (CFD) relies heavily on robust, low-dissipative numerical scheme. For implicit large eddy simulation (ILES) under-resolved scales are accounted for by a properly shaped subgrid-scale model inherent in a nonlinear numerical scheme [1]. Schranner *et al.* [2] have optimized the truncation error of a Weighted Essentially Non-Oscillatory (WENO) scheme to initiate physically consistent transition of an under-resolved Taylor-Green Vortex (TGV) flow and recover the Kolmogorov inertial subrange in its turbulent state. Targeted ENO (TENO) schemes have been proposed by [3] to overcome the deficiencies of WENO schemes, e.g. excessive dissipation for lower-order schemes, order degeneration, and limited robustness for central-biased or very high-order schemes. Similar to WENO schemes, TENO schemes offer shaping of the inherent effective local dissipation and dispersion by a set of free parameters. Fu *et al.* [3] have optimized TENO schemes based on the approximated dissipation-dispersion condition (ADC) proposed in [4]. ADC builds upon the approximate dispersion relation (ADR) [5] derived for linear analysis. Hence, nonlinear shock-capturing schemes optimized with ADC, may not necessarily transfer optimal behavior to physical flow problems that incorporate a range of interacting scales.

Data-driven methods for shaping numerical schemes for CFD, and especially Neural-Networks (NN)-based ones have gained momentum recently and proven to be beneficial. E.g. Bezgin *et al.* [6] have constructed a 3rd order low-dissipation scheme WENO3-NN where each stencil weight is computed based on a trained neural network. Some drawbacks of NN are the need for a large number of training data or the need for careful hyperparameters selection. By contrast, Bayesian optimization (BO) is a data-driven method for optimization that relies on a limited number of trials and does not require derivative information, i.e. it is highly efficient while providing solutions of high confidence. Design optimization (DO) methods have been introduced to shape nonlinear numerical schemes for ILES in [2], thereby, the design objective of shaping a WENOCU6-M1 scheme to predict physically consistent inertial subrange scaling has been followed. Winter *et al.* [7] have further-developed the DO approach by employing BO to the same optimization problem. Their work [7] has shown that BO performs superior to the DO approach of [2]. Nevertheless, their work is limited to weakly compressible flows and a two-dimensional optimization problem. Comparing with WENOCU6-M1, TENO not only provides free parameters to optimize the nonlinear dissipation, yet, also provides adjustability to the linear weights, allowing to optimize the inherent dissipation of the background linear scheme. Hence, TENO, when shaped accordingly is superior to WENOCU6-M1 for compressible flows and may also be superior for vortical or turbulent flows.

In this work, we use BO to explore whether the $5^{th}$ order TENO scheme, denoted as TENO5, can be optimized for underresolved compressible flows that include discontinuities and a range of interacting scales.

This paper is structured as follows: In Section 2, the two essential elements for BO, Gaussian process regression (GPR) and expected improvement (EI), are introduced. A brief review of TENO5 and the effects of its free parameters are given in Section 3. The objectives and optimization configuration can be found in Section 4. Finally, the optimization results are presented and benchmark test cases are studied in Section 5.

## 2 BAYESIAN OPTIMIZATION

BO has two elements: a probabilistic surrogate model and an acquisition function. As a probabilistic surrogate model, a GPR is chosen in this work due to its robustness and analytical tractability [8, 9]. As an acquisition function, the expected hypervolume improvement is used; it generates a candidate sample by balancing the location of the expected optimum and area of high model uncertainty of the surrogate model [10].

### 2.1 Gaussian Process Regression

Assuming an unknown noise-free scalar function $f(\mathbf{x})$ with $\mathbf{x} \in \mathbb{R}^d$ denoting a bounded $d$-dimensional input parameter space and $f \in \mathbb{R}$ denoting a scalar output space and given a finite set of $n$ input samples $\mathbf{X} = \{\mathbf{x}_i | i = 1,2,...,n\}$ drawn in the input space and their corresponding evaluations $\mathbf{f} = \{f(\mathbf{x}_i) | i = 1,2,...,n\}$ in the output space, a training set shall be $\mathcal{D} = (\mathbf{X}, \mathbf{f})$. Based on $\mathcal{D}$, a GPR model can be written as [8]

$$\hat{\mathbf{f}}(\mathbf{X}) \sim \mathcal{N}(m(\mathbf{X}); K(\mathbf{X},\mathbf{X})), \tag{1}$$

where $m(\mathbf{X})$ and $K(\mathbf{X},\mathbf{X})$ denote the mean function and the $n \times n$ covariance matrix, respectively. The latter evaluates the covariance function $k(\mathbf{x},\mathbf{x}') = E[(f(\mathbf{x}) - m(\mathbf{x}))(f(\mathbf{x}') - m(\mathbf{x}'))]$ at all possible pairs of input vectors in $\mathbf{X}$. $m(\mathbf{x}) = 0$ can be assumed [8].

The covariance function $k(\mathbf{x},\mathbf{x}')$ is chosen such that with increasing distance $r = |\mathbf{x},\mathbf{x}'|$, $f(\mathbf{x})$ and $f(\mathbf{x}')$ correlate less. Within this work, the radial basis function (RBF) kernel $k(\mathbf{x},\mathbf{x}') = \theta_o exp\left(-\frac{r^2}{2l^2}\right)$ is used. $l$ is the length scale and $\theta_o$ a weighting factor which expresses the output scale or signal variance [8]. They are hyperparameters of the covariance function and denoted by $\theta = (l, \theta_o)$ within the following.

Let $\mathbf{x}_*$ denote an arbitrary trial for $\hat{f}$, its predictive mean and covariance function are:

$$\mu(\mathbf{x}_*) = \mathbf{k}(\mathbf{x}_*, \mathbf{X}) K(\mathbf{X},\mathbf{X})^{-1} \mathbf{f} \tag{2}$$

and

$$\sigma^2(\mathbf{x}_*) = k(\mathbf{x}_*,\mathbf{x}_*) - \mathbf{k}(\mathbf{x}_*,\mathbf{X}) K(\mathbf{X},\mathbf{X})^{-1} \mathbf{k}(\mathbf{X},\mathbf{x}_*). \tag{3}$$

To determine the optimal set of hyperparameters $\theta$, the marginal log likelihood (MLL) of $\hat{\mathbf{f}}(\mathbf{X})$

$$log\ p(\hat{\mathbf{f}}|\mathbf{X},\theta) = -\frac{1}{2}\mathbf{f}^T \cdot K(\mathbf{X},\mathbf{X})\mathbf{f} - \frac{1}{2} log|K(\mathbf{X},\mathbf{X})| - \frac{n}{2} log(2\pi) \tag{4}$$

is maximized. For this purpose, the Adam optimizer [11, 12] is employed. The converged $\hat{f}(\mathbf{x})$ is denoted as the posterior distribution or the surrogate model of $f(\mathbf{x})$.

### 2.2 Expected Improvement

A GPR model provides an approximate interpolation of the real function $f(\mathbf{x})$ by a normal distribution of the prediction at an arbitrary point $\mathbf{x}_*$, i.e. $f(\mathbf{x}_*) \sim \mathcal{N}\left(\mu(\mathbf{x}_*); \sigma^2(\mathbf{x}_*)\right)$. To effectively and efficiently find the optimum of $f(\mathbf{x})$, further samples may need to be drawn, thereby approaching the location of the expected optimum and reducing the model uncertainty of the GPR $\hat{f}(\mathbf{x})$. Given a maximization scenario, samples are drawn sequentially, and selected based on maximizing the expected improvement, i.e.[10]

$$\mathbf{x}_{ct} = argmax\ EI(\mathbf{x}). \tag{5}$$

with $EI(\mathbf{x}) = E\left[max(\hat{f}(\mathbf{x}) - f_n^*, 0)\right]$ where $f_n^*$ is the currently best output. This equation expresses the expectation of the improvement comparing to the current optimum considering the variance of $\hat{f}(\mathbf{x})$. In this work, a sequential least squares programming method [13] is used to solve Eq. (5).

## 3 BRIEF REVIEW OF TARGETED ENO SCHEME

In this section the Euler equations and their discretization are introduced. Subsequently, a description of the TENO5 scheme is provided. Thereby, the free parameters of TENO5 and their contribution to the scheme inherent dissipation and dispersion are discussed.

### 3.1 Numerical-Flux Formulation and Discretization

The Euler equations, without source terms, read in vector notation

$$\frac{\partial \mathbf{U}}{\partial t} + \nabla^T \cdot \mathbf{F}(\mathbf{U}) = 0, \tag{6}$$

with

$$\mathbf{U} = \begin{bmatrix} \rho \\ \rho\mathbf{u} \\ E \end{bmatrix}, \quad \mathbf{F}(U) = \begin{bmatrix} \mathbf{u}\rho \\ \rho\mathbf{u} \otimes \mathbf{u} + p\mathbf{I} \\ \mathbf{u}(E+p) \end{bmatrix} \tag{7}$$

being the vector of conservative states and the convective flux vector, respectively. Therein, $\rho$ denotes the density, $t$ the time, $\mathbf{u}$ the velocity vector, $p$ the pressure, $\mathbf{I}$ the identitiy matrixd and $E = \rho e + 1/2\rho\mathbf{u}\cdot\mathbf{u}$ the total energy with the internal energy $\rho e$ and the kinetic energy $1/2\rho\mathbf{u}\cdot\mathbf{u}$. We employ the ideal equation-of-state $p = (\gamma - 1)\rho e$, where $\gamma$ denotes the ratio of specific heats, to close the system of equations. We employ a finite-volume approach using cuboid finite volumes

$$\frac{d}{dt}\bar{\mathbf{U}}_i = \frac{1}{\Delta x}\left(\mathbf{F}_{i-\frac{1}{2},j,k} - \mathbf{F}_{i+\frac{1}{2},j,k} + \mathbf{G}_{i,j-\frac{1}{2},k} - \mathbf{G}_{i,j+\frac{1}{2},k} + \mathbf{H}_{i,j,k-\frac{1}{2}} - \mathbf{H}_{i,j,k+\frac{1}{2}}\right) \tag{8}$$

where $\Delta x$ denotes the cell size, and $\mathbf{F}$, $\mathbf{G}$, and $\mathbf{H}$ are the approximate cell-face fluxes in $x-$, $y-$, and $z-$ direction, respectively. We obtain the convective fluxes by solving the Riemann problem at cell faces using a Roe Riemann solver [14]. To advance the solution in time, we employ a third-order Runge-Kutta Total Variation Dimishing scheme [15]. We apply the low-dissipative high-order TENO5 reconstruction scheme to stably recover discontinuities and entire range of scales of the considered flow problems.

### 3.2 Fifth-order Targeted ENO Weighting

To construct a cell-face value according to the TENO framework [3], in a first step, $r$ sub stencils $\hat{f}_{n,i+\frac{1}{2}}$ with $n = 0,...r-1$ are constructed from neighboring cell-averaged states. The target cell-face value $\hat{f}_{i+\frac{1}{2}}$ of order $(2r-1)$ is obtained in a second step, by a weighted addition of the $r$ sub-stencils, i.e. $\hat{f}_{i+\frac{1}{2}} = \sum_{k=0}^{r-1} w_k\, \hat{f}_{k,i+\frac{1}{2}}$. To achieve an ENO-like behaviour, a stencil which contains a discontinuity is suppressed. Within this work, a fifth-order TENO scheme, i.e. $r = 3$, denoted as TENO5 is used. The three sub-stencils are:

$$\begin{aligned} \hat{f}_{0,i+\frac{1}{2}} &= \tfrac{1}{6}\left(-f_{i+1} + 5f_i + 2f_{i+1}\right), \\ \hat{f}_{1,i+\frac{1}{2}} &= \tfrac{1}{6}\left(2f_{i-2} - 7f_{i-1} + 11f_i\right), \\ \hat{f}_{2,i+\frac{1}{2}} &= \tfrac{1}{6}\left(2f_i + 5f_{i+1} - f_{i+2}\right). \end{aligned} \tag{9}$$

To determine the weights, the smoothness measures [16, 17]

$$\gamma_k = \left( C + \frac{\tau_5}{\beta_k + \varepsilon} \right)^q, k = 0, 1, 2, \tag{10}$$

are evaluated, where $\tau_5 = |\beta_1 - \beta_2|$ is the global reference smoothness indicator and $\varepsilon$ is a small value to prevent division by zero. $C$ and $q$ are two integer parameters that are free parameters. $\beta_k$ are the smoothness indicators for each sub-stencil and listed in [3]. The three smoothness measures are normalized according to $\chi_k = \gamma_k / \sum_{k=0}^{2} \gamma_k$ and compared to the cutoff parameter $C_T$ such that

$$\delta_k = \begin{cases} 0, & if\ \chi_k < C_T, \\ 1, & otherwise. \end{cases} \tag{11}$$

Finally, the nonlinear weights $w_k$ are expressed in terms of the linear weights $d_k$ as $w_k = d_k \delta_k / \sum_{k=0}^{2} d_k \delta_k$. Note that, if $\delta_k \equiv 1$ for all $k = 0, 1, 2$ and one chooses the ideal linear weights $d_0 = 0.6, d_1 = 0.3, d_2 = 0.1$, a 5th order upwind scheme is obtained.

### 3.3 The free Parameters of TENO5

The linear-combination of the sub-stencils determines the TENO5 dissipation and dispersion properties. Hence, by adjusting the weights $d_k$, the dissipation-dispersion relation is optimizable. TENO5 can be divided into a 4th-order upwind-biased and a 4th-order central-biased sub-scheme [3]

$$\begin{aligned} g^u_{i+\frac{1}{2}} &= \tfrac{1}{12} \left( f_{i-2} - 5 f_{i-1} + 13 f_i + 3 f_{i+1} \right), \\ g^c_{i+\frac{1}{2}} &= \tfrac{1}{12} \left( -f_{i-1} + 7 f_i + 7 f_{i+1} - f_{i+2} \right), \end{aligned} \tag{12}$$

respectively. A higher order scheme is constructed by assembling these according to

$$f^{5^{th}}_{i+\frac{1}{2}} = \eta g^u_{i+\frac{1}{2}} + (1 - \eta) g^c_{i+\frac{1}{2}}, \tag{13}$$

with $\eta$ expressing the bias towards the upwind scheme. Choosing $\eta = 0.4$ leads to the original TENO5 scheme [3]. By selecting $\eta = 0.2$, Fu *et al.* [3] have constructed a TENO5 scheme that has beneficiary dissipation-dispersion properties based on the ADC, see Section 1. In this work, we denote this TENO5 scheme as $\text{TENO5}_{\text{adc}}$.

The parameters $C$ and $q$, see Eq. (10) control the extent the stencil smoothness is being taken into account. Thus, a large $C$ entails minimal influence of the smoothness metric $\tau_5 / (\beta_k + \varepsilon)$ of the stencils, which in the limit leads to recovery of the linear scheme with no nonlinear dissipation, thereby, the bias towards a central or upwind-scheme depends on the choice of $\eta$. If $q$ is large, minor non-smoothness of a stencil may lead to its exclusion. Consequently, the three free parameters $C$, $q$, and $\eta$ are used for shaping optimal TENO5 schemes.

## 4 OPTIMIZATION OBJECTIVES AND CONFIGURATION

TENO5 in its formulations proposed in [3] behaves overly dispersive for intermediate and high wavenumbers in compressible flows, and overall excessively dissipative to be useful as a subgrid model for LES [18, 19]. In this work, we make use of BO to explore its optimal formulations for compressible flows with gasdynamic discontinuities and fluid-dynamic instabilities as well as turbulent or vortex flows. In this section, the optimization objectives are defined and the optimization configuration is detailed.

### 4.1 Optimization Objective for TENO5$_{\text{comp}}$

To optimize a TENO5 scheme for compressible flows with gasdynamic discontinuities and fluid-dynamic instabilities relevant to compressible flows, i.e. to state TENO5$_{\text{comp}}$, the Sod shock tube [20] is used as a training test case. The Sod shock tube is defined by the initial condition of

$$(\rho, u, p) = \begin{cases} (1.0, 0.0, 1.0) & if\ 0 \leq x < 0.5, \\ (0.125, 0.0, 0.1) & otherwise. \end{cases} \tag{14}$$

It is simulated in a domain of $[0,1]$ with 40 uniform cells until a time of $t_{end} = 0.2$. Then, the distributions of $\rho$, $u$, and $p$ are compared to an analytical solution, i.e. the capability of a scheme to recover the analytical solution is investigated. Since $\rho$, $u$, and $p$ vary in magnitude, these are normalized by corresponding minimum and maximum values of the initial simulations. The optimization objective can be defined on basis of the normalized $\rho$, $u$, and $p$ as

$$o_{comp} = \sum_{s} \left\| s_{sim} - s_{ref} \right\|_2, \ s = \rho, u, p, \tag{15}$$

where $s_{sim}$, and $s_{ref}$ denote the simulation, and analytical data for $\rho$, $u$, and $p$, respectively, $\|\cdot\|_2$ denotes the L2 norm.

### 4.2 Optimization Objective for TENO5$_{\text{iles}}$

To optimize a TENO5-scheme for vortex flows or turbulent flows, i.e. to state TENO5$_{\text{iles}}$, the TGV at an infinite Reynolds number as in [2, 7] serves as the test cases. A TGV develops from the initial laminar condition

$$\begin{aligned} \rho &= 1.0 \\ (u, v, w) &= (sin(x)cos(y)cos(z), -cos(x)sin(y)cos(z), 0.0) \\ p &= 100 + \frac{1}{16}[(cos2x + cos2y)(x + cos2z) - 2] \end{aligned} \tag{16}$$

to a 3D, isotropic turbulent flow, decaying self-similarly only if the numerical model permits proper evolution [2]. For the TGV, a cubic domain with $\triangle x = \frac{2\pi}{64}$ is used. At $t = 10$, the difference between the numerically simulated Kolmogorov scaling inertial subrange $E(k_i)$ and the theoretical one, defined as

$$o_{iles} = \left\| \log E(k_i) - \log A k_i^{-5/3} \right\|_2, \qquad i = r, r+1, ..., s \tag{17}$$

is measured. $r = 3$ and $s = 33$ mark the first and last wave number of the inertial subrange. $Ak_i^{-5/3}$ is the reference Kolmogorov inertial subrange. Evaluation of this objective requires the value of $A$, which differs from sample to sample. The regression analysis described in [2] is used to determine $A$.

### 4.3 Optimization Configuration

TENO5$_{\text{comp}}$ is intended for compressible flow simulations. While keeping the non-linear dissipation contribution from non-smooth stencils as low as necessary, spurious oscillations originating from such shall be suppressed, i.e. $C$ and $q$ shall be rather small. While $\eta = 0.2$ entails minimal dissipation [3] and $\eta = 0.4$ recovers the original TENO5, that is excessively dissipative, a value of $\eta$ favorable to the use for compressible flow simulations is expected in between. Consequently, the values for $q$, $C$, and $\eta$ shall be

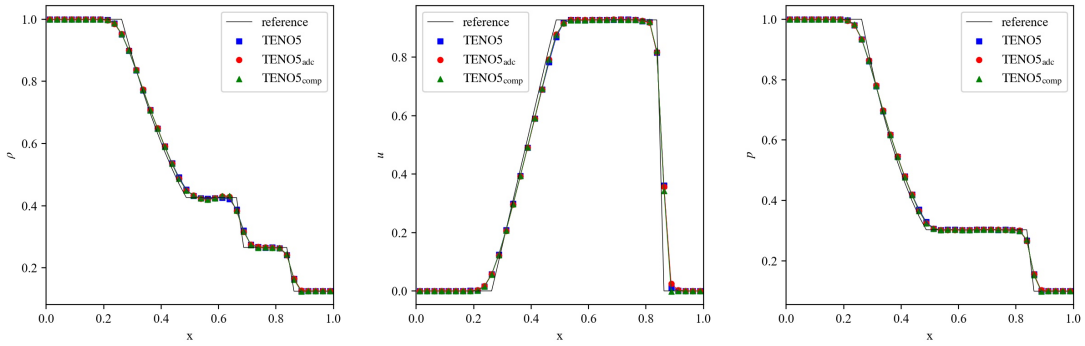


(a) (b) (c)

Figure 1: The (a) density, (b) velocity and (c) pressure profiles of Sod's shock tube simulated with TENO5, $\text{TENO5}_{\text{adc}}$ and $\text{TENO5}_{\text{comp}}$ schemes.

within $[1,10]$, $[1,100]$ and $[0.2,0.4]$ for $o_{comp}$, respectively. Note that we use $\Delta(q,C,\eta) = (1,1,0.001)$ for $o_{comp}$.

$\text{TENO5}_{\text{iles}}$ shall be favorable for underresolved simulations of vortex flows. $\text{TENO5}_{\text{adc}}$ is too dissipative for ILES to model the under-resolved scales [18], hence, $\eta \leq 0.2$ favors a rather central-biased TENO5 scheme. According to [2, 7] $C$ and $q$ are $[1,20]$, and $[1000,20000]$, respectively, for the WENOCU6-M1 scheme. TENO5 can provide more dissipation than WENOCU6-M1, thus, by means of a large $C$, non-linear dissipation shall be reduced. By means of screening, a range of values for $C$ has been determined. Overall, the values of $q$, $C$, and $\eta$ are within $[1,20]$, $[1000,60000]$, and $[0.0,0.2]$ for $o_{iles}$, respectively. Note that we use $\Delta(q,C,\eta) = (1,1000,0.001)$ for $o_{iles}$.

For the Bayesian Optimization of $\text{TENO5}_{\text{comp}}$ and $\text{TENO5}_{\text{iles}}$ 20 initial samples are drawn from the three-dimensional input parameter space using a Sobol-sequence [7, 9]. Employing the GPBO process outlined in Section 2, 30 optimization iterations are passed. ALPACA [21, 22], an MPI-parallelized C++ framework for complex flow simulations is used to run the test cases. The Ax-platform [23], combining the GP regression modeling implemented in GPyTorch [24] and the BO of BoTorch [25] is used for the GPBO.

## 5 OPTIMIZATION RESULTS AND BENCHMARKING

### 5.1 Optimization Results

The optimal parameters for $\text{TENO5}_{\text{comp}}$ have been determined as $(q,C,\eta) = (6,3,0.311)$. Figure 1 shows the distribution of $\rho$, $u$, and $p$ for the Sod shock tube as simulated with TENO5, $\text{TENO5}_{\text{adc}}$, $\text{TENO5}_{\text{comp}}$, and the analytical reference solution, respectively. For $\text{TENO5}_{\text{comp}}$, the discontinuities are resolved sharply without degenerating the smoothness of other regions. $\text{TENO5}_{\text{comp}}$ improves to TENO5 in the three dimensions $\rho$, $u$, and $p$ of $o_{comp}$ by 6.33%, 9.67%, and 6.30%, respectively. The optimal parameters for $\text{TENO5}_{\text{iles}}$ have been determined as $(q,C,\eta) = (13,56000,0.1)$. Figure 2 shows the turbulent kinetic energy spectrum of the TGV in its turbulent state as simulated with TENO5, $\text{TENO5}_{\text{adc}}$, $\text{TENO5}_{\text{iles}}$, and for reference, the Kolmogorov inertial subrange spectrum. As indicated in Figure 2, TENO5 and $\text{TENO5}_{\text{adc}}$ are excessively dissipative, while $\text{TENO5}_{\text{iles}}$ does fulfill the design goal of re-

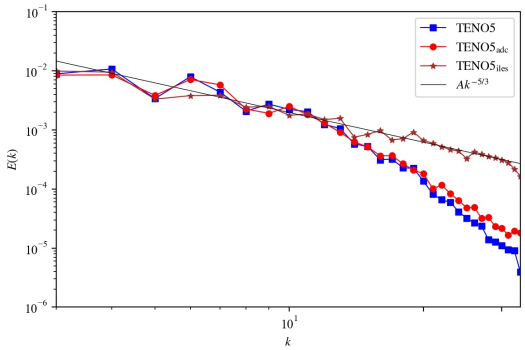


Figure 2: Turbulent kinetic energy spectrum of TGV with TENO5, $\text{TENO5}_{\text{adc}}$ and $\text{TENO5}_{\text{iles}}$

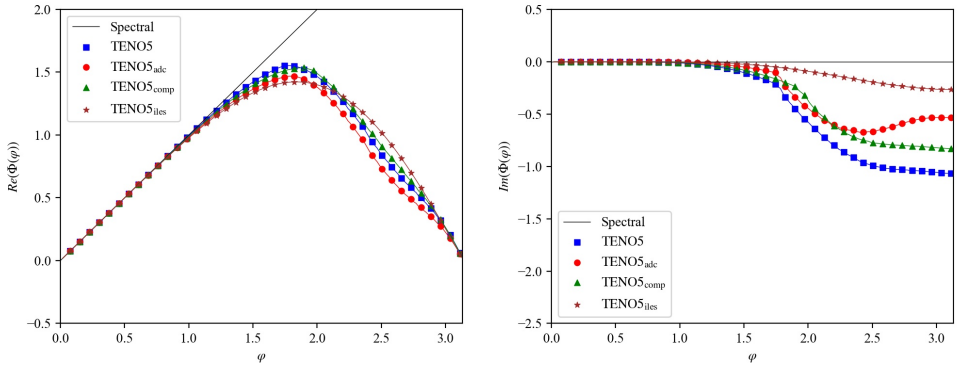


(a) (b)

Figure 3: The spectral properties for TENO5, $\text{TENO5}_{\text{adc}}$, $\text{TENO5}_{\text{comp}}$ and $\text{TENO5}_{\text{iles}}$. (a) presents the dispersion, the real part of the $\Phi(\varphi)$, and (b) presents the dissipation, the imaginary part of the $\Phi(\varphi)$.

covering the Kolmogorov-scaling inertial subrange spectrum well. $o_{iles}$ has been evaluated for TENO5, and $\text{TENO5}_{\text{adc}}$ as 10.82, and 8.92, respectively; it is 1.19 for $\text{TENO5}_{\text{iles}}$.

Figure 3 presents the spectral properties of dispersion and dissipation according to [5], for TENO5, $\text{TENO5}_{\text{adc}}$, $\text{TENO5}_{\text{comp}}$ and $\text{TENO5}_{\text{iles}}$. While $\text{TENO5}_{\text{comp}}$ outperforms $\text{TENO5}_{\text{adc}}$ significantly in terms of the dispersion error it is more dissipative than $\text{TENO5}_{\text{adc}}$ in the higher wave number range. $\text{TENO5}_{\text{comp}}$ and TENO5 indicate a similar dispersivity, yet, $\text{TENO5}_{\text{comp}}$ is less dissipative. $\text{TENO5}_{\text{iles}}$ compares in terms of dispersion properties to $\text{TENO5}_{\text{adc}}$ for low wave numbers, yet, for higher wave numbers the dispersive error is lowest for $\text{TENO5}_{\text{iles}}$. Out of the compared TENO5 family members the dissipative error, especially for high wave numbers, is least for $\text{TENO5}_{\text{iles}}$.

### 5.2 Benchmark tests

Within the following, the performance of the TENO5 schemes is studied with selected benchmark tests. With 5.2.1, and 5.2.2 we demonstrate the superiority of the $\text{TENO5}_{\text{comp}}$ scheme that has a reduced - when compared to TENO5 and $\text{TENO5}_{\text{adc}}$ and properly balanced dispersive and dissipative error for

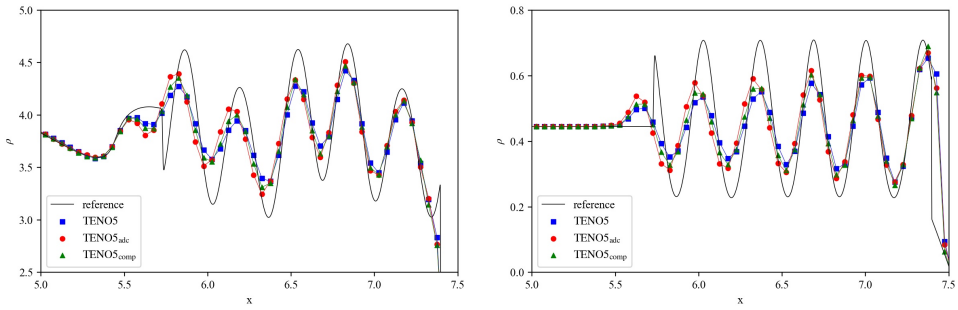


(a) (b)

Figure 4: Shu-Osher problem simulated with TENO5, TENO5$_{\text{adc}}$ and TENO5$_{\text{comp}}$: (a) density; (b) entropy.

flow phenomena common to compressible flows.

### 5.2.1 Shu-Osher Problem

The Shu-Osher [26] problem is an ideal one-dimensional test case to study the "shock-capturing and wave-resolution capability" [3] of a scheme. Given the initial conditions

$$(\rho, u, p) = \begin{cases} (3.857, 2.629, 10.333) & if\ 0 \leq x < 1, \\ (1 + 0.2sin(5x), 0, 1) & if\ 1 \leq x \leq 10. \end{cases} \tag{18}$$

the flow is simulated in a domain discretized with 200 uniform cells until $t_{end} = 1.8$. Figure 4 shows the density and entropy field in those part of the domain most relevant to indicating the performance in "shock-capturing and wave-resolution capabilities" [3] of high-order numerical schemes. Comparing the simulation of the oscillation in the region of $5.5 \leq x \leq 6.5$, the amplitude error of TENO5$_{\text{adc}}$ in comparison to TENO5, and TENO5$_{\text{comp}}$ is lowest, yet, the phase error of TENO5$_{\text{comp}}$ is significantly lower than for TENO5$_{\text{adc}}$.

### 5.2.2 2D Implosion

The 2D implosion originating from the initial conditions

$$(\rho, u, v, p) = \begin{cases} (0.125, 0, 0, 0.14), & if\ (x+y) < 0.15, \\ (1.0, 0, 0, 1.0), & otherwise. \end{cases} \tag{19}$$

as proposed in [27] serves to study the capabilities of a numerical scheme to robustly simulate Richtmyer-Meshkov instabilities, one of the common types of fluid-dynamic instabilities. Thereby, robustly implies that the solution is not deteriorated due to instabilities originating from numerical errors when resolution is limited. Note that in ALPACA the numerical symmetry-preserving techniques proposed in [28] is employed. The domain is bounded by $[0, 0.3] \times [0, 0.3]$ with fully symmetric boundaries and discretized by $160 \times 160$ uniform cells. Figure 5 shows the simulation results as obtained with TENO5, TENO5$_{\text{adc}}$ and TENO5$_{\text{comp}}$, respectively. Comparing the plume and the lower left corner of Fig. 5a to Figs. 5b, 5c, only

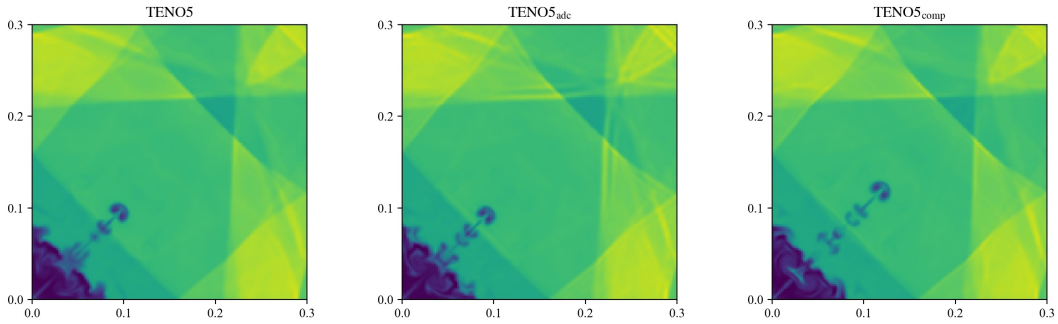


(a) (b) (c)

Figure 5: The density distribution (from 0.4 to 1.1) of implosion text case simulated by (a) TENO5, (b) $\text{TENO5}_{\text{adc}}$ and (c) $\text{TENO5}_{\text{comp}}$ at end time $t = 2.5$.

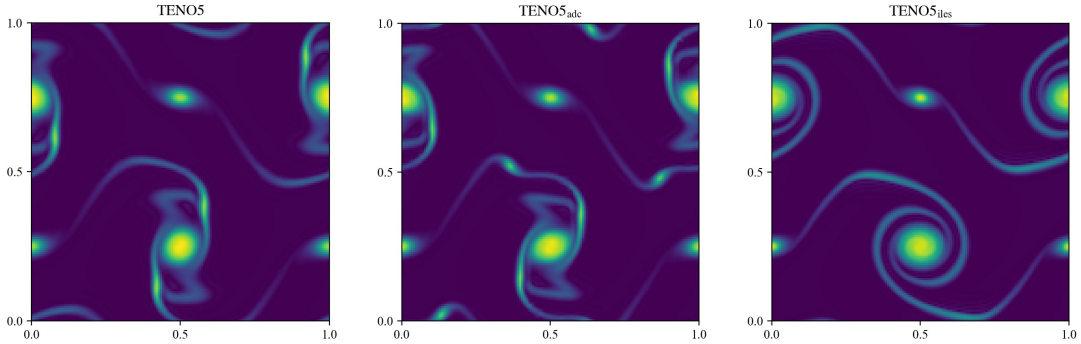


(a) (b) (c)

Figure 6: The absolute vorticity field (from 0 to 65) of 2D free shear flow with a thin layer simulated by (a) TENO5, (b) $\text{TENO5}_{\text{adc}}$ and (c) $\text{TENO5}_{\text{iles}}$ at t=1.0.

larger scales can be observed and the plume is shorter, which is due to the dominating dissipative error of TENO5. Also, $\text{TENO5}_{\text{adc}}$ entails spurious oscillations at the reflected shock waves, most visible shock distortions appear at the interacting shocks. We attribute these spurious oscillations to the excessively dispersive error behavior of $\text{TENO5}_{\text{adc}}$. A well-resolved and a long plume with no apparent spurious oscillation in the vicinity of the reflecting or interacting shocks is produced with $\text{TENO5}_{\text{comp}}$.

### 5.2.3 2D Free Shear Flow with Thin Layer

To benchmark $\text{TENO5}_{\text{iles}}$, a thin-layer 2D free shear flow is studied. It originates from the initial condition of [29]

$$(\rho, u, v, p) = \begin{cases} (1.0, tanh(\theta(y-0.25)), \delta sin(2\pi x), 100.0) & if\ y \leq 0.5, \\ (1.0, tanh(\theta(0.75-y)), \delta sin(2\pi x), 100.0) & otherwise, \end{cases} \tag{20}$$

where $\theta = 100$ is the shear layer width and $\delta = 0.05$. The domain is bounded by $[0,1] \times [0,1]$ with periodic boundaries and discretized underresolvedly with $160 \times 160$ uniform cells. The Reynolds number is 10000. Figure 6 shows the absolute vorticity field simulated by TENO5, TENO5$_{\text{adc}}$ and TENO5$_{\text{iles}}$ at $t = 1.0$, respectively. As a direct consequence of an overly dissipative scheme, spurious vortices form. An excessivly dispersive scheme would, in later stages lead to numerical instabilities. Due to the excessive dissipation of TENO5 and TENO5$_{\text{adc}}$ the primary vortices are distorted, while TENO5$_{\text{iles}}$ resolves the primary vortex properly. The spiral structure in the core of the primary vortex layer roll-upp is well represented, which is in line with the diminishing dispersive error of TENO5$_{\text{iles}}$.

## 6 CONCLUSIONS

The GPBO approach has been employed to efficiently develop TENO5-based schemes that balance the dissipation and dispersion as required for specific types of flows. These schemes are particularly advantageous for underresolved simulations of either compressible flows with gas dynamic discontinuities and instabilities, as well as vortex or turbulent flows. For these optimizations, two appropriate optimization objectives have been defined. On the one hand, the Sod shock tube test flow poses the objective for compressible schemes to resolve a discontinuity sharply while concurrently being as little as possible adversely effected to dispersive errors. On the other hand, the TGV delivers the basis for the objective of properly transitioning a flow from a laminar to a turbulent state with a proper Kolmogorov inertial subrange and thus a proper subgrid-scale model for implicit large eddy simulations.

With a selected set test flows, the specialized TENO5 schemes are benchmarked. Thereby, we note that the optimizations are robust in the sense that both optimal schemes are superior to the original TENO5 schemes of Fu *et al.* [3] for test flows incorporating the fluid-dynamic phenomena on basis of which an optimization has been conducted. In practice, they also deliver improved results when applied to other flow types that have not been used to define the optimization objectives.

## REFERENCES


[1] Adams, N.A., Hickel, S. and Franz, S. Implicit subgrid-scale modeling by adaptive deconvolution. *Journal of Computational Physics*. (2004) **39**:821-841.

[2] Schranner, F.S., Rozov, V. and Adams, N.A. Optimization of an Implicit Large-Eddy Simulation Method for Underresolved Incompressible Flow Simulations. *AIAA Journal*. (2016) **5**:5.

[3] Fu, L., Hu, X.Y. and Adams, N.A. A family of high-order targeted ENO schemes for compressible-fluid simulations. *Journal of Computational Physics* (2016). **305**:333-359.

[4] Hu, X.Y., Tritschler, V.K., Pirozzoli, S. and Adams, N.A. Dispersion-dissipation condition for finite difference schemes. *arXiv:1204.5088 [physics.flu-dyn]*. (2014).

[5] Pirozzoli, S. On the spectral properties of shock-capturing schemes. *Journal of Computational Physics*. (2006) **219**:489-497.

[6] Bezgin, D.A., Schmidt, S.J. and Adams, N.A. WENO3-NN: A maximum-order three-point data-driven weighted essentially non-oscillatory scheme. *Journal of Computational Physics*. (2022) **452**:110920.

[7] Winter, J.M., Schranner, F.S. and Adams, N.A. Iterative Bayesian optimization of an implicit les method for under-resolved simulations of incompressible flows. *10th International Symposium on Turbulence and Shear Flow Phenomena*. (2017).

[8] Rasmussen, C.E. and Williams, C.K.I. *Gaussian Processes for Machine Learning*. the MIT Press,

(2006).

[9] Feng, Y., Schranner, F.S., Winter, J.M. and Adams, N.A. A Multi-Objective Bayesian Optimization Environment for Systematic Design of Numerical Schemes for Compressible Flow. *SSRN*. (2022).

[10] Jones, D.R., Schonlau, M. and Welch, W.J. Efficient global optimization of expensive black-box functions. *Journal of Global Optimization*. (1998) **13(4)**:455–492.

[11] Kingma, D.P. and Ba, J. Adam: A Method for Stochastic Optimization. *arXiv*. (2014)

[12] Loshchilov, I. and Hutter, F. Decoupled Weight Decay Regularization. *International Conference on Learning Representations*. (2019)

[13] Byrd, R.H., Lu, P. and Nocedal, J. A Limited Memory Algorithm for Bound Constrained Optimization. *SIAM Journal on Scientific and Statistical Computing*. (1995) **16(5)**: 1190-1208.

[14] Roe, P. L. Approximate Riemann solvers, parameter vectors, and difference schemes. *Journal of computational physics*. (1981) **43(2)**:357-372.

[15] Gottlieb, S., and Shu, C. W. Total variation diminishing Runge-Kutta schemes. *Mathematics of computation of the American Mathematical Society*. (1998) **67(221)**:73-85.

[16] Hu, X.Y. and Adams, N.A. Scale separation for implicit large eddy simulation. *J. Comput. Phys.* (2011) **230**:7240-7249.

[17] Borges, R., Carmona, M., Costa, B. and Don, W.S. An improved weighted essentially non-oscillatory scheme or hyperbolic conservation laws. *J. Comput. Phys.* (2008) **227**:3191=3211.

[18] Fu, L., Hu, X.Y. and Adams, N.A. Implicit large eddy simulations with a high-order TENO scheme. *10th International Symposium on Turbulence and Shear Flow Phenomena*. (2017).

[19] Fu, L., Hu, X.Y. and Adams, N.A. Implicit large eddy simulations with a high-order TENO scheme. *10th International Symposium on Turbulence and Shear Flow Phenomena*. (2017).

[20] Sod, G.A. A survey of several finite difference methods for systems of nonlinear hyperbolic conservation laws. *J. Comput. Phys.* (1978) **27**:1-31.

[21] Hoppe, N., Winter, J.M., Adami, S. and Adams, N.A. ALPACA - a level-set based sharp-interface multiresolution solver for conservation laws. *Computer Physics Communications*. (2022) **272**:108246.

[22] Hoppe, N., Adami, S. and Adams, N.A. A parallel modular computing environment for three-dimensional multiresolution simulations of compressible flows. *Computer Methods in Applied Mechanics and Engineering*. (2022) **391**:114486.

[23] Daulton, S., Balandat, M. and Bakshy, E. Differentiable Expected Hypervolume Improvement for Parallel Multi-Objective Bayesian Optimization. *arXiv*. (2020).

[24] Gardner, J.R., Pleiss G., Bindel, D., Weinberger, K.Q. and Wilson, A.G. GPyTorch: Blackbox Matrix-Matrix Gaussian Process Inference with GPU Acceleration. *arXiv*. (2018).

[25] Balandat, M., Karrer, B, Jiang, D.R., Daulton, S., Letham, B., Wilson, A.G. and Bakshy, E. BoTorch: A Framework for Efficient Monte-Carlo Bayesian Optimization. *arXiv*. (2019).

[26] Shu, C.W. and Osher, S. Efficient Implementation of Essentially Non-oscillatory Shock-Capturing Schemes, II. *Upwind and High-Resolution Schemes*. (1989).

[27] Liska, R. and Wendroff, B. Comparison of Several difference schemes on 1D and 2D Test problems for the Euler equations. *SIAM Journal on Scientific Computing*. (2003) **25**:995-1017.

[28] Fleischmann, N., Adami S. and Adams, N.A. Numerical symmetry-preserving techniques for low-dissipation shock-capturing schemes. *Journal of Computational Physics*. (2019) **189**:94-107.

[29] Minion, M.L. and Brown, D.L. Performance of Under-resolved Two-Dimensional Incompressible Flow Simulations, II, *Journal of Computational Physics*. (1997) **138**:734-765.